Nonlinear Analysis of a Two-Parachute System Undergoing Pendulum Motion

Jing Pei*
NASA Langley Research Center, Hampton, Virginia, 23681

Motion resembling that of a pendulum undergoing large-amplitude limit cycle oscillation was observed during a series of flight tests of an unoccupied Orion Capsule Parachute Assembly System (CPAS) comprised of two parachutes and a capsule payload. Large excursions away from vertical by the capsule could cause it to strike the ground or ocean at a large angle with respect to vertical, or at a large horizontal speed. These conditions are undesirable because they would endanger the occupants of the capsule in an actual mission. A simplified planar dynamics model in conjunction with a nonlinear normal force coefficient vs. angle of attack model serves as the basis of an analytical investigation of the fundamental dynamics of this pendulum motion. Output error methodology from system identification theory was used to identify the parameters of the nonlinear aerodynamics model. The identified model yielded excellent comparison with portions of flight test data where the pendulum motion occurred. Due to the inherent nonlinear nature of the pendulum motion limit cycle, traditional nonlinear analysis techniques were applied to gain further insight into the system. Lyapunov's direct method provided mathematical proof in the absolute stability of the pendulum mode. Describing Function method was used to predict the amplitude and frequency of the limit cycle oscillation. Finally, phase plane analysis allowed easy visualization on the size and shape of the limit cycle with respect to variations in key aerodynamic parameters.

I. Introduction

As discussed in Ref. [1], a series of flight tests was conducted to characterize the performance of the Orion Multi Purpose Crew Vehicle (MPCV) parachute cluster. It is apparent from flight tests that the two-parachute cluster/capsule system can undergo limit-cycle pendulum motion with large excursions from vertical by the payload. The pendulum motion can result in the capsule striking the ground at a large angle with respect to vertical, or at a large horizontal speed, both of which are highly undesirable. In Ref. [1] Ray and Machín describe the pendulum motion observed during flight testing and summarize a series of studies performed in an attempt to understand the causes of the phenomenon. The pendulum motion was not observed with the nominal three-main parachute configuration. In Ref. [2] Ali and etc. summarized series of efforts taken by the Orion CPAS program on understanding and mitigating the two-parachute cluster pendulum problem. The Program ultimately accepted the risks involved with the pendulum motion associated with the two-parachute configuration and opted not to alter the design of the parachutes which would diminish the performance of the nominal three-parachute configuration.

Over the past 50 years, a number of analytical, numerical, and experimental investigations have been performed with the goal of understanding parachute pitch-plane dynamics (for example, Refs. [3]–[6]). Ref. [7] used CFD to study the stability of various main parachute configurations from the Apollo and MPCV programs. It was demonstrated that an increase in the porosity of the parachute improved its stability characteristics hence reduced the severity of the pendulum motion. Figure 1 are representative plots of normal force and axial force coefficients comparing a stable vs. unstable main parachute configuration. It is apparent from the C_N vs. α plot that unstable configuration has a negative slope at $\alpha = 0$ and two stable

*Aerospace Engineer, Vehicle Analysis Branch

equilibrium points at $\pm\alpha_o$. As described in Ref. [7], by adding a "gap" in the parachute (increase porosity), the C_N slope becomes close to zero at $\alpha = 0$ and is considered the stable configuration. In addition, the two stable α_o shift closer to $\alpha = 0$. However, this modification comes at a cost in the reduction of the axial force coefficient which results in a higher descent velocity. Ref. [6] and [8] provides similar insights regarding the flow physics associated with non-porous vs. porous configurations and how it affects the parachute stability characteristics.

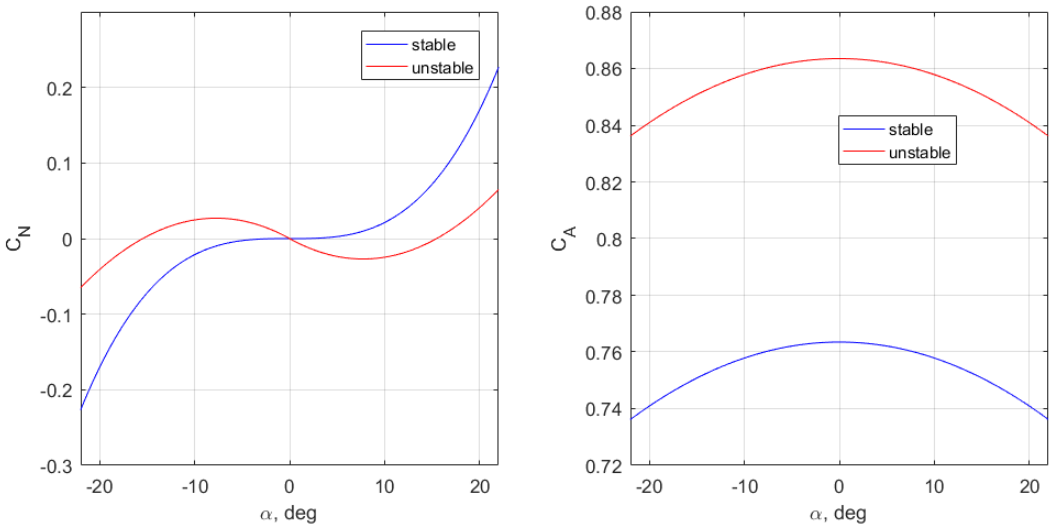

Figure 1. C_N and C_A coefficients representative of unstable vs. stable parachute configurations

The current study focuses on the unstable MPCV main parachute design (modeled by the red curves in Fig. 1) which it is highly susceptible to the pendulum motion under the two-main cluster configuration. A planar dynamics model was developed[9] to capture the fundamental characteristics of the pendulum motion. Subsequently, the output-error method from system identification theory[10] was applied to portions of the two-parachute flight test data that exhibited pendulum motion. The identified planar aerodynamics model along with the dynamics model produced excellent comparison with flight data. Due to the inherent nonlinear nature of the pendulum motion; nonlinear analysis techniques[11] including Lyapunov's direct method, Describing Function method, and phase plane analysis were used to analyze the system to provided further insight into the pendulum limit cycle oscillation. To the author's knowledge, this is the first time a nonlinear pendulum dynamic model has been used with system identification techniques to model pendulum motion of the CPAS cluster composed of two-parachutes and a payload. Important note: the paper does not address the mechanism that triggers the pendulum motion for the two-parachute configuration. It appears to be a non-planar phenomenon and is still an area of active research.

The remainder of the paper is organized as follows. A simplified planar model of the system is presented in Sec. II and used as the basis for an analytical study of the fundamental dynamics of pendulum motion. In Sec. III, the output-error method from system identification theory was applied to portions of flight data that exhibited pendulum motion and key parameters in the nonlinear aerodynamics model were extracted. Section IV illustrates application of traditional analysis techniques for nonlinear system to provide further insight into pendulum motion. Conclusions are presented in Sec. V. **Note: Due to ITAR (International Tariff and Arms Regulation) restrictions, all aerodynamic parameters shown in this paper are placeholders. Y-axis labels have been removed for figures with flight data.**

II. Planar Model

Despite this is a multi-body system in real life, Ref. [9] shows a planar dumbbell model is adequate in capturing the underlying dynamics of the pendulum motion. The dumbbell model is illustrated in Fig. 2. The capsule is modeled as a particle rather than an extended rigid body and aerodynamic forces acting on the capsule were ignored.[3] The two parachutes are treated as a single particle. The rigid body B contains

two particles. Particle P_C has a mass of m_C, the total mass of two parachutes, which includes dry mass as well as the mass of air trapped in each of the canopies. Particle P_L has a mass of m_L and represents the capsule. Body B moves such that P_C and P_L remain at all times in a plane fixed in a Newtonian reference frame N. A right-handed set of mutually perpendicular unit vectors $\hat{\mathbf{n}}_1$, $\hat{\mathbf{n}}_2$, and $\hat{\mathbf{n}}_3$ is fixed in N. Unit vectors $\hat{\mathbf{n}}_1$ and $\hat{\mathbf{n}}_3$ lie in the plane in which motion takes place, and are directed as shown in Fig. 2; $\hat{\mathbf{n}}_1$ is horizontal, $\hat{\mathbf{n}}_2$ is directed into the page, and $\hat{\mathbf{n}}_3$ is vertical, directed downward. A right-handed set of mutually perpendicular unit vectors $\hat{\mathbf{b}}_1$, $\hat{\mathbf{b}}_2$, and $\hat{\mathbf{b}}_3$ is fixed in B. Unit vectors $\hat{\mathbf{b}}_1$ and $\hat{\mathbf{b}}_3$ are directed as shown in Fig. 2; $\hat{\mathbf{b}}_1$ has the same direction as the position vector $\mathbf{r}^{P_C P_L}$ from P_C to P_L. Unit vector $\hat{\mathbf{b}}_2$ is directed into the page; note that it is fixed in N as well as in B. Further details of the dumbbell model can be found in Ref. [9].

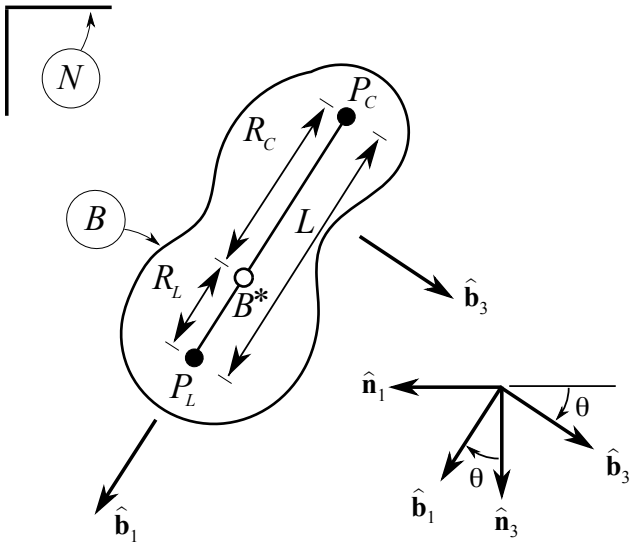

Figure 2. Rigid Body Containing Two Particles.

The translational and rotational degrees of freedom (DOF) were derived in Ref. [9] and shown in Eqs. 1 and 2:

$$ {}^{N}\mathbf{a}^{B^\star} = \frac{1}{m_C + m_L}\Big\{ -\left[A_x \sin\theta + A_z \cos\theta\right]\hat{\mathbf{n}}_1 + \left[W_C + W_L - A_x \cos\theta + A_z \sin\theta\right]\hat{\mathbf{n}}_3 \Big\} \tag{1} $$

$$ \ddot{\theta} + \frac{1}{m_C L}\left[\left(m_C\, g - W_C\right)\sin\theta - A_z\right] = 0 \tag{2} $$

A_x, the resultant of the aerodynamic axial forces applied to the two parachutes, can be expressed as:

$$ A_x = 2 q_\infty S_{\text{ref}} C_A \tag{3} $$

where q_∞ is the dynamic pressure, S_{ref} is the reference area of a single parachute, and C_A is the drag coefficient for a single parachute. A_z, the resultant of the aerodynamic normal forces applied to the two parachutes, can be expressed as:

$$ A_z = -2 q_\infty S_{\text{ref}} C_N \tag{4} $$

C_N is the aerodynamic normal force coefficient for a single parachute. C_A and C_N are nonlinear functions of α, the instantaneous angle of attack of the parachute, shown below. α can be approximated as the sum of the swing angle, θ, with the induced angle of attack at the parachute location, $\frac{R_C \dot{\theta}}{V_\infty}$. In keeping with traditional aerodynamic definitions, C_A is applied in the direction of $-\hat{\mathbf{b}}_1$, and C_N is applied in the direction of $-\hat{\mathbf{b}}_3$.

$$ C_A = C_{A_o} + \frac{1}{2} C_{A_\alpha} \alpha_o \left(\frac{\alpha^2}{\alpha_o^2} - 1\right) \tag{5} $$

$$ C_N(\alpha) = \frac{C_{N_\alpha}}{2\alpha_o^2}\left(\alpha^3 - \alpha_o^2 \alpha\right) \tag{6} $$

III. Output-Error Results

The first CPAS drop test with two main parachutes that exhibited significant pendulum motion was CDT 3-11.[1,2] According to Ref. [2], a third of the way into the full open portion of the main parachute flight, the system developed a swinging motion of about 15 deg in amplitude, and increased up to 24 deg as it approached the ground. During the pendulum motion, the system was translating towards the Northeast due to the direction of the wind as it descended. The parachute cluster appears to have aligned its "weak" axis with the direction of the wind. Ref. [1] defines the "weak" axis being parallel with the wind direction and orthogonal to the plane of oscillation that contains the two parachutes. The motion can be approximated as planar in nature; hence Eqs. 1 and 2 should be adequate in capturing the gross characteristics of the pendulum motion.

The output-error method,[10] widely used in parameter estimation for aircrafts was applied to the pendulum portion of the CDT 3-11 flight data. To perform the optimization, the routine called **oe.m** in the SIDPAC toolbox[12] was used. The vector of parameters to be estimated was:

$$\Theta = [C_{A_o} \quad C_{A_\alpha} \quad \alpha_o \quad C_{N_\alpha} \quad C_{N_{\dot{\alpha}}}] \tag{7}$$

The aerodynamic model structures shown in Eq. 5 and 6 are based on previous studies[3,4,6,7] and not identified from the flight data. An additional damping term, $C_{N_{\dot{\alpha}}}$ was added to Eqs. (6) to account for unsteady time lag effects in the rotational degree-of-freedom.[9,13] The MPCV aerodynamic database suggests that for the pendulum motion to occur, an unstable value of $C_{N_{\dot{\alpha}}}$ is required. The measurements from the flight data to match are: θ (swing angle), $V_{\mathrm{n_3,air}}$ (air relative velocity in the Down direction), $V_{\mathrm{lat,air}}$ (root-sum-square of the air relative velocity in North and East directions). System parameters used in the planar dynamics model are recorded in Table 1.

Table 1. System Parameters.

parameter	value	units
S_{ref} (single parachute)	10563	ft^2
L	235	ft
Capsule Weight, W_L	21906	$\mathrm{lb_f}$
Dry Weight of Two Parachutes, W_C	656	$\mathrm{lb_f}$
Total Mass of Two Parachutes, (dry and entrapped air), m_C	614	slugs
Distance from System Center of Mass to Capsule CM, R_L	114	ft

Winds act as the sole source of excitation to the two-parachute cluster system. In the flight data, the best estimated winds are provided in the North, East, and Down directions. For it to be used in the planar dynamics model, the flight winds in the North and East directions were resolved along the plane of the pendulum oscillation as shown in Fig. 3. Output-error analysis converged within 80 iterations. Figure 4 shows comparison between the output-error model with the flight data. Other than the initial amplitude mismatch during the first 15 seconds or so, the identified planar model appears to provide an excellent match with flight data in the swing angle time history. The fundamental frequency (η Hz) of the swing angle is virtually identical between the identified model with the flight data. The model swing angle amplitude is within 20% of the flight. $V_{\mathrm{lat,air}}$ also shows good comparisons as well. The slightly larger differences in $V_{\mathrm{n_3,air}}$ is likely due to the lack of best estimated winds in the Down direction. Consider the drastic simplification of the actual system dynamics (18 DOF, flexible riser lines, non-rigid parachutes, etc.), it is remarkable that the planar dumbbell model can adequately predict the fundamental characteristics of the pendulum motion.

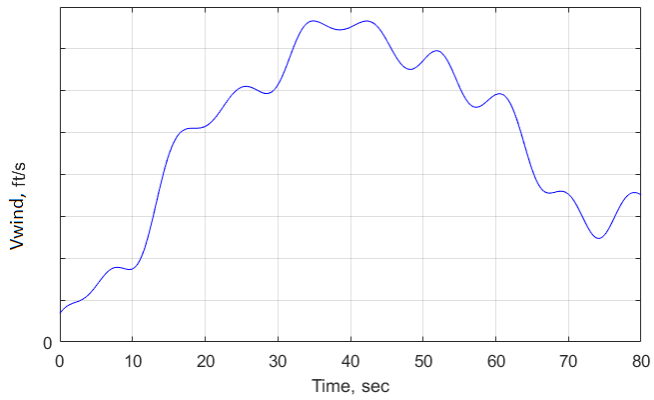

Figure 3. CDT 3-11 Flight Winds

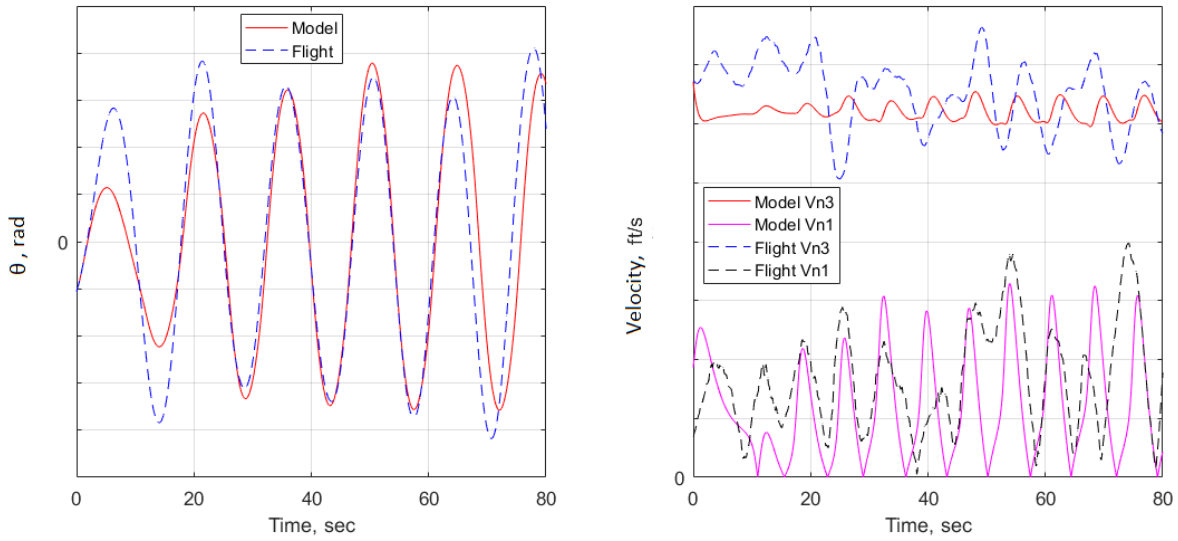

Figure 4. Output-error model with CDT 3-11 Flight Data

Table 2 shows the parameter estimation results from the output-error method. The estimated parameters and the their standard errors are listed in columns 2 and 3, respectively. The standard errors were corrected for colored residuals using the **m_colores.m** function in SIDPAC.[12] $C_{N_{\dot{\alpha}}}$ is positive ($C_{Z\dot{\alpha}}$ negative) and therefore dynamically unstable as expected. Figures 5 to 7 are comparisons between the identified C_N, $C_{N_{\dot{\alpha}}}$, and C_A vs. α models with the current MPCV aerodynamic database. For the static C_N model, the trends are similar, with the database showing a greater value for α_o but a shallower slope of C_N at α_o (smaller restoring force). For the damping derivative, the model indicates a constant $C_{N_{\dot{\alpha}}}$ whereas the database shows variations with α. Furthermore, the model shows a significantly higher value of $C_{N_{\dot{\alpha}}}$ (more dynamic instability). For C_A, the database and the model show similiar trends with the database having a constant value of C_A between $\alpha = \pm\alpha_o$.

Table 2. Parameter Estimation Results from CDT 3-11

parameter	$\hat{\Theta}$	s($\hat{\Theta}$)
C_{A_o}	0.8	0.05
C_{A_α} (rad^{-1})	-0.2	0.1
α_o (rad)	0.3	0.1
C_{N_α} (rad^{-1})	0.4	0.1
$C_{N_{\dot{\alpha}}}$ (rad/s)$^{-1}$	1.5	0.3

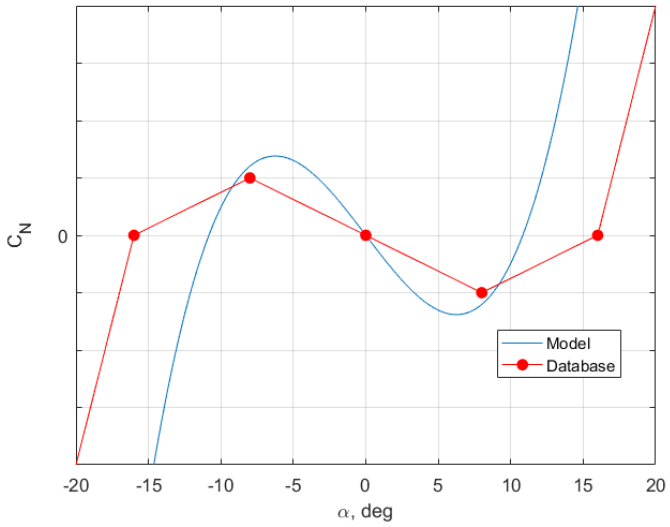

Figure 5. C_N vs. α, identified model vs. MPCV database

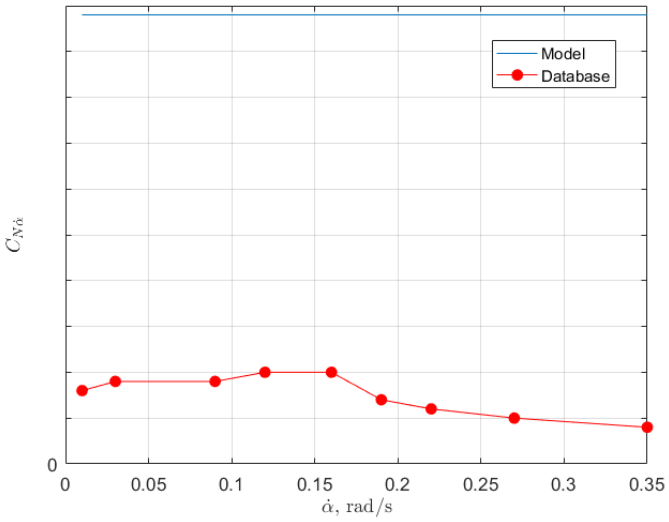

Figure 6. $C_{N\dot{\alpha}}$ vs. α, identified model vs. MPCV database

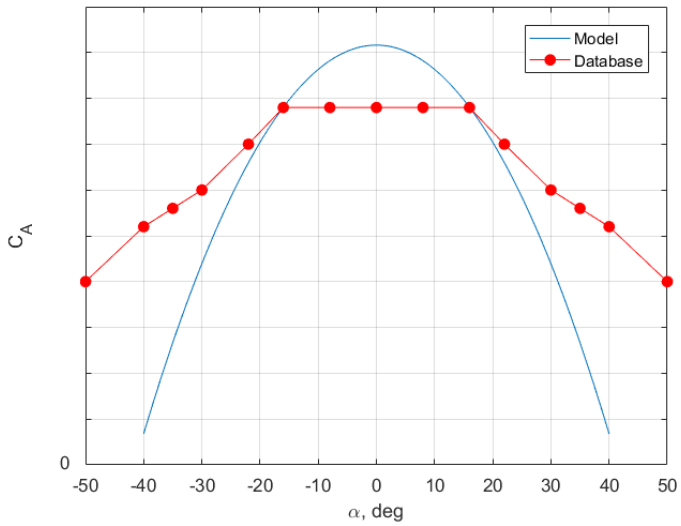

Figure 7. C_A **vs.** α**, identified model vs. MPCV database**

The parameters identified from the CDT 3-11 flight shown in Table 2 were used to predict the pendulum motion from the CDT 3-12 flight. According to Ref. [2], during the CDT 3-12 drop test the pendulum motion occurred almost immediately after full inflation of the main parachutes and gradually increased to an amplitude of approximately 24 deg until impact. Similar to the CDT 3-11 flight, the system was also translating towards the Northeast due to the direction of the winds as it descended. Figure 8 shows the CDT 3-12 flight winds resolved in the plane of the pendulum oscillation. Figure 9 shows the comparison between the model identified from CDT 3-11 flight with CDT 3-12 flight data. Once again, other than the initial amplitude mismatch, the identified planar model appears to provide an excellent match with flight data in the swing angle time history. Both model and flight data shows the swing angle fundamental frequency to be η Hz while error in the amplitude of oscillation is within 10%. $V_{\mathrm{n_3,air}}$ and $V_{\mathrm{lat,air}}$ shows good comparisons as well.

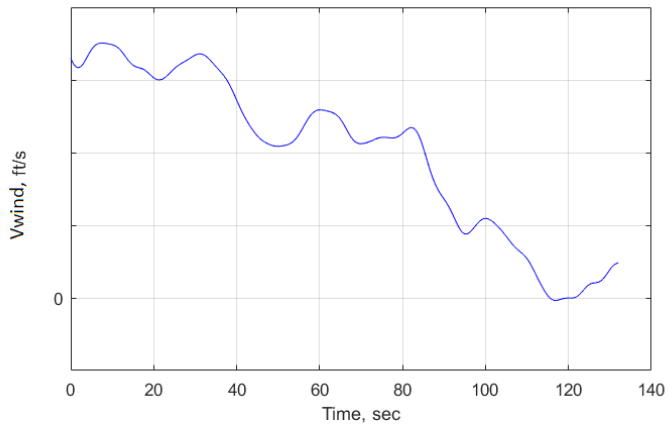

Figure 8. CDT 3-12 Flight Winds

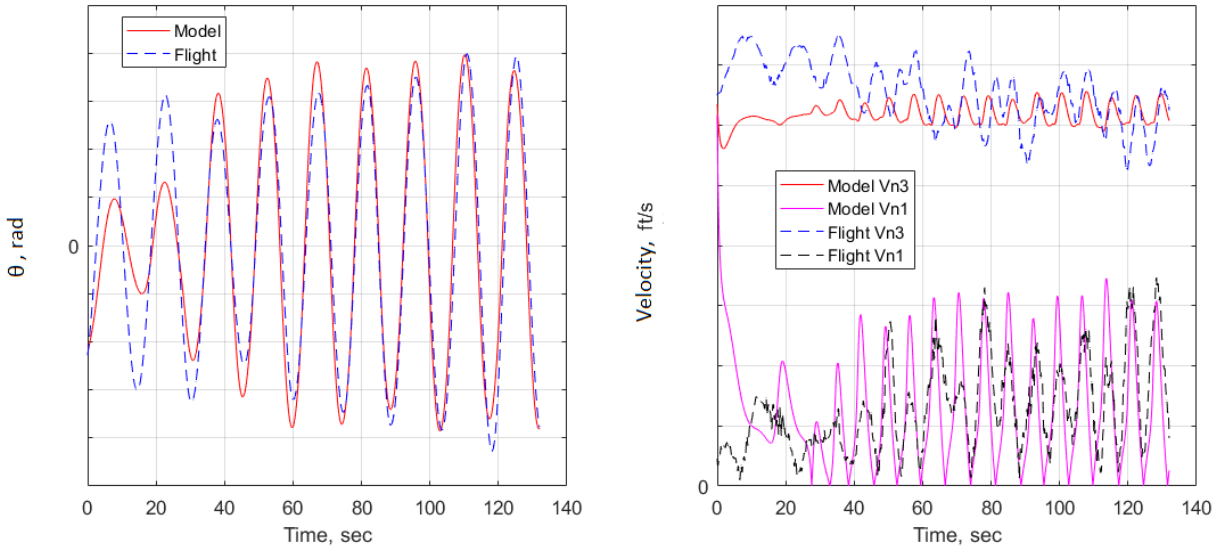

Figure 9. Output Error Model with CDT 3-12 Flight Data

It is apparent that the identified planar dumbbell model appears to do a remarkable job in matching the underlying dynamics of the pendulum motion in both the CDT 3-11 and 3-12 flight data. However, its limitation should be re-emphasized. The dumbbell model is not capable of producing some of the more complicated behaviors (such as the maypole and flyout motions) observed during the CDT 3-02 and 3-08 flights in which the pendulum motion did not occur.[1,2] The model also does not predict how pendulum motion is triggered. This appears to be a non-planar phenomenon that is highly dependent on the gradient of the wind direction and magnitude. It is still a topic of ongoing research.

Finally, the current model does not provide much insight into why a cluster of three parachutes is more resistant towards the pendulum motion compare to a cluster of two. According to Ref. [1], CDT 3-07 involved three parachutes. Pendulum motion was observed during a brief interval in which the configuration of the parachutes changed from the usual triangular arrangement to a collinear one with coincident projections of all three parachutes onto the plane parallel to the wind direction. The oscillations damped out after the parachutes regained their triangular configuration. Equations 1 to 6, therefore, are applicable in the case of pendulum motion with three parachutes, with the following modifications: 1) W_C and m_C are the dry weight and total mass of three parachutes. 2) A coefficient of 3 replaces 2 in Eqs. 3 and 4.

IV. Nonlinear Analysis

The pendulum mode associated with the two-parachute capsule system is inherently a nonlinear phenomenon. In this section, several well-known techniques are used to analyze the nonlinear system.[11] The first is the phase plane analysis that allows one to visualize the system trajectories on a two-dimensional plane. The second is the Describing Function (DF) method which approximates the nonlinear system as a linear "equivalent" and applies an extension of the frequency response technique. The DF technique is extremely useful in predicting the amplitude and frequency of limit cycle oscillations. Finally, Lyapunov's direct method allows formulation of a scalar energy-like function that allows a mathematical proof in the stability of the pendulum mode.

A. Phase Plane

The second-order nature of the pendulum mode makes it an excellent system for phase plane analysis. Figure 10 shows the phase portraits of θ and α for several initial conditions that are inside, outside, and in close proximity of the limit cycle curve. The trajectories all eventually converge to the closed orbit. It is also apparent from Fig. 1 that the system has an unstable equilibrium point at the origin. Hence, for initial conditions in the vicinity of the unstable origin would cause the system to be repelled towards the limit cycle

orbit. Figure 11 shows the phase portraits of θ and α with a 25% reduction in the identified value of C_{N_α}. The reduction in the restoring force at high α results in a slight increase in the amplitude of the limit cycle oscillation.

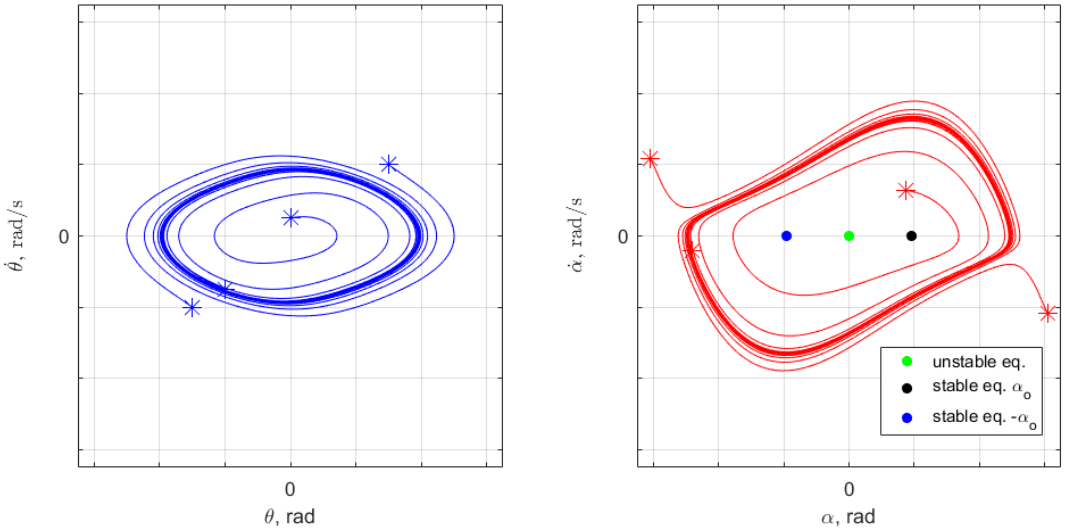

Figure 10. Representation of the Pendulum Limit Cycle on a Phase Plane

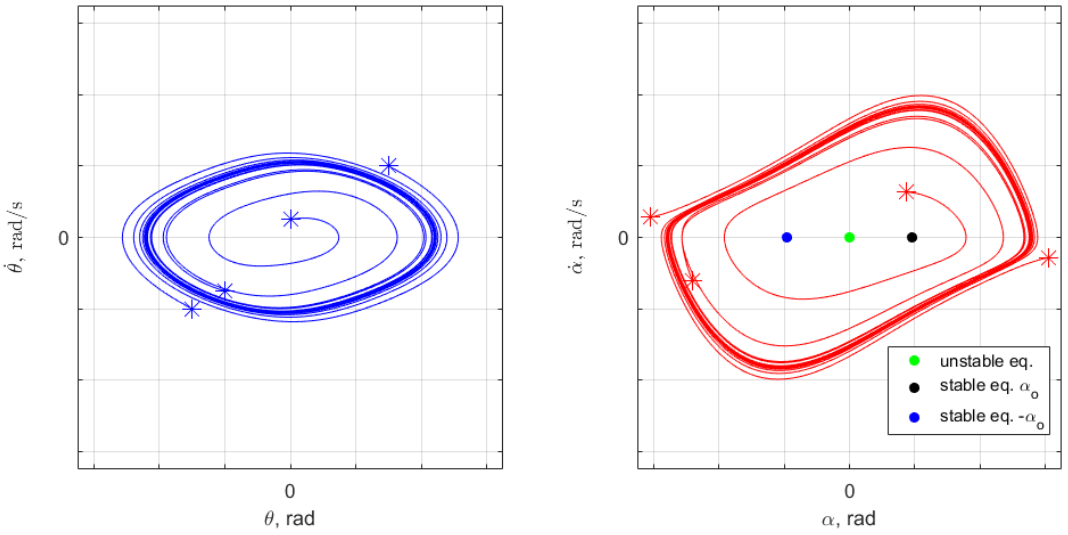

Figure 11. Representation of the Pendulum Limit Cycle on a Phase Plane, 25% reduction in C_{N_α}

Note: there exist sub-regions on the α phase plane where the initial disturbance is small enough such that the system settles on to one of the stable equilibrium points, $\pm\alpha_o$ (while θ converges to zero). These special cases not considered because the paper strictly focuses on the pendulum motion after it has developed. Figure 12 shows the phase portrait of θ and α for a parachute configuration with a stable C_N vs. α profile (same $C_{N_{\dot{\alpha}}}$ value). The amplitude of the swing angle limit cycle is reduced by a factor greater than 2 compare to Fig. 10. This observation is consistent with description on parachute stability in Ref. [6]. It states in reality both systems are unstable; however in the parachute community the one with substantial amplitude of oscillation is considered unstable while the other is regarded as stable.

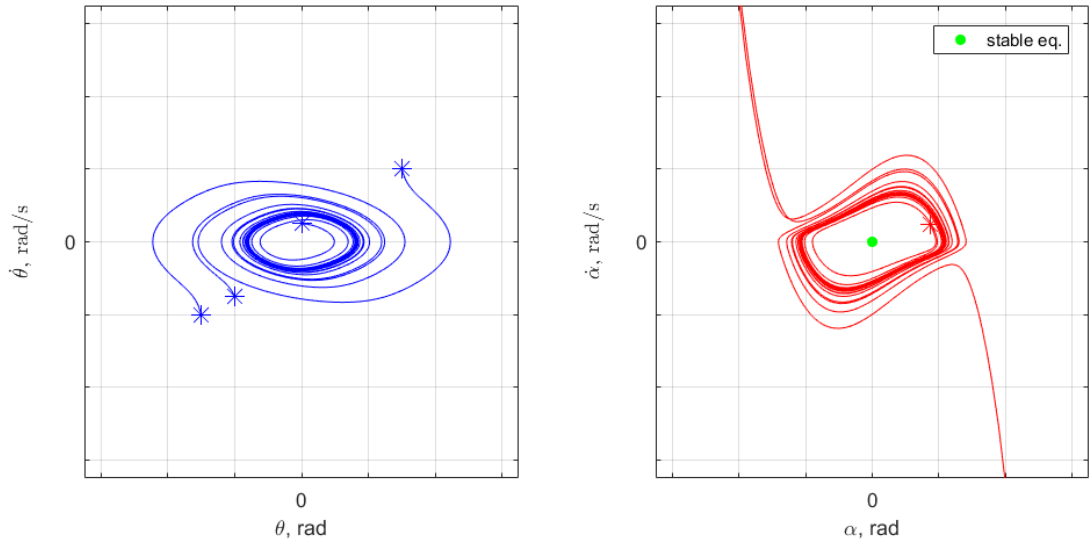

Figure 12. Representation of the Pendulum Limit Cycle on a Phase Plane, Stable Configuration

B. Describing Function

The Describing Function (DF) method is an approximate linear technique for analyzing nonlinear systems. It is an extension of the frequency response method for nonlinear systems. Unlike Lyapunov methods, DF method does not hinge on the success of a trial-and-error search for a Lyapunov function and its main purpose is to predict the amplitude and frequency of oscillation of limit cycles in nonlinear systems.[11] Figure 13 is a general depiction of the DF block diagram. It requires the nonlinear system to be separated by its linear and nonlinear components.

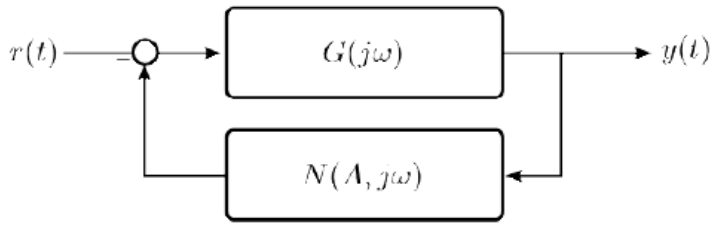

Figure 13. Describing Function Block Diagram

The premise of the DF method is that there exists a limit cycle in the system in the form of:

$$x(t) = A\sin(\omega t) \tag{8}$$

where A is the limit cycle amplitude and the ω being the frequency. The closed-loop characteristic equation of the system can be represented as:

$$G(j,\omega)N(A,\omega) + 1 = 0 \tag{9}$$

where $G(j,\omega)$ is the frequency response of the linear component and $N(A,\omega)$ is the approximate frequency response of the nonlinear portion. $N(A,\omega)$ is the complex ratio of the fundamental component of the nonlinear element given a sinusoidal input, ignoring the higher-frequency harmonics (characteristic associated with nonlinear systems[11]). Unlike the traditional frequency response for a linear system, the describing function of a nonlinear element is dependent on its amplitude, A.[11] Equation 9 can be re-written as:

$$G(j,\omega) = -\frac{1}{N(A,\omega)} \tag{10}$$

Generally, one would graph both sides of the Eq. 10 on the complex plane and look for intersection points. There are an infinite number of intersection points; however, only the intersection points with matched ω indicates the possible existence of limit cycles. To analyze the pendulum mode limit cycle oscillation, the rotational dynamics is of particular interest. Equation 2 can be re-written as:

$$\ddot{\theta} + \frac{2q_\infty S_{\text{ref}} C_{N_{\dot{\alpha}}}}{m_C L}\dot{\theta} + \frac{m_C g - w_C}{m_C L}\sin\theta + \frac{2q_\infty S_{\text{ref}}}{m_C L} C_N(\alpha) = 0 \tag{11}$$

C_N is a cubic function with α as shown in Eq. 6 and $\sin\theta$ can be representated in its Taylor Series expansion form:

$$\sin\theta = \theta - \frac{\theta^3}{6} + \frac{\theta^5}{120} + ... \tag{12}$$

The angle of attack at the parachute location can be approximated as the sum of the swing angle, θ, with the induced angle of attack:

$$\alpha = \theta + \frac{R_C\dot{\theta}}{V_\infty} \tag{13}$$

Substitute Eq. 6 to 13 into Eq. 11, the rotational dynamics can be re-written strictly as a function of θ and $\dot{\theta}$ and can be separated into linear and nonlinear components required for DF analysis:

$$\begin{aligned}\underbrace{\ddot{\theta} + \frac{2q_\infty S_{\text{ref}}}{m_C L}\Big[C_{N_{\dot{\alpha}}} - \frac{C_{N_\alpha} R_C}{2V_\infty}\Big]\dot{\theta} + \Big[\frac{m_C g - w_C}{m_C L} + \frac{q_\infty S_{\text{ref}}}{m_C L} C_{N_\alpha}\Big]\theta}_{\text{Linear}} + \\ \underbrace{\Big[-\frac{m_C g - w_C}{6 m_C L}\theta^3 + \frac{q_\infty S_{\text{ref}} C_{N_\alpha}}{m_C L \alpha_o^2}(\theta + \frac{R_C\dot{\theta}}{V_\infty})^3\Big]}_{\text{Nonlinear}} = 0\end{aligned} \tag{14}$$

$N(A,\omega)$ is computed by passing a series of sinusoidal inputs, $u(t)$ in the form shown in Eq. 8 through the nonlinear element which has output, $q(t)$, consisting of higher harmonics. Once $q(t)$ has reached a period solution, the last two periods are used to compute the Fourier integrals:[14]

$$a_1 = \frac{1}{\pi}\int_{-\pi}^{\pi} q(t)\cos(\omega t) d(\omega t) \tag{15}$$

$$b_1 = \frac{1}{\pi}\int_{-\pi}^{\pi} q(t)\sin(\omega t) d(\omega t) \tag{16}$$

The magnitude and phase of $N(A,\omega)$ can be determined from the Fourier coefficients:

$$|N| = \frac{\sqrt{a_1^2 + b_1^2}}{A} \tag{17}$$

$$\phi(N) = \tan^{-1}\left(\frac{a_1}{b_1}\right) \tag{18}$$

According to the CDT 3-11 flight data, the amplitude of the limit cycle is around 0.3 rad with a frequency of η Hz. With that in mind, the amplitude range of $q(t)$ used for the DF analysis is kept between 0.2 to 0.36 rad with a frequency range of η_L Hz to η_H Hz. The frequency response of $G(j,\omega)$ and $-1/N(A,\omega)$ are plotted on a Nyquist diagram for a range of values of A as shown in Fig. 14.

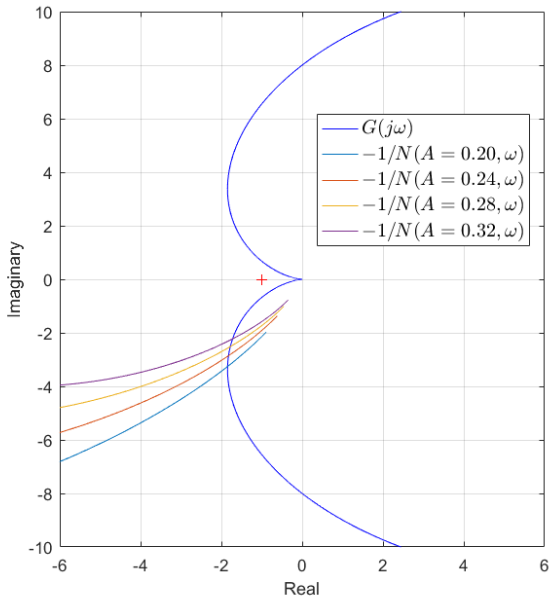

Figure 14. Describing Function Analysis

Figure 14 shows multiple intersection locations between $G(j\omega)$ with $-1/N(A,\omega)$; however, the one with matched frequency occurs at $A = 0.24$ rad and $\omega = \zeta$ rad/s. The DF analysis predicts the pendulum limit cycle oscillation with a period of approximately T sec and an amplitude of 0.24 rad. The predicted period of oscillation is identical to the flight data and model as shown in Fig. 4. The 25% difference in the amplitude can be explained by the coupling of the translational and rotational dynamics as well as the inherent approximations associated with the DF method. Figure 15 shows the discrete Fourier transform of the model θ time history shown in Fig. 4. It has a fundamental frequency of η Hz, the second harmonic at η_2 Hz, and the third harmonic at η_3 Hz. Only the fundamental frequency is retained in the DF analysis.

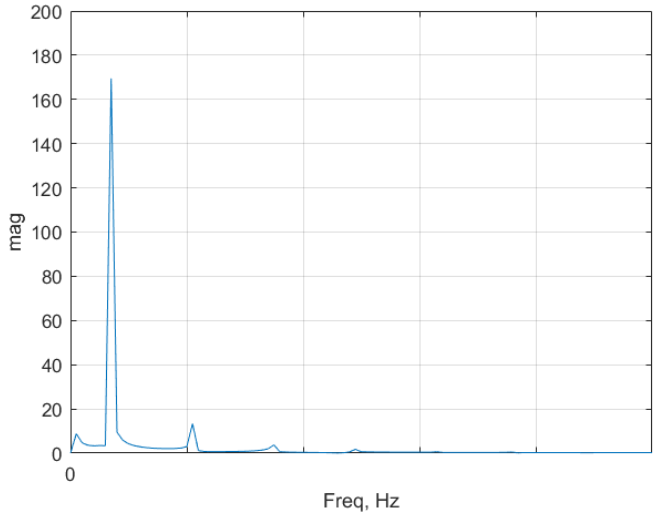

Figure 15. Discrete Fourier Transform

C. Lyapunov's Direct Method

Lyapunov's direct method is the mathematical extension of a fundamental physical observation: if the total energy of a system is continuously dissipated, then the system, whether linear or nonlinear, must eventually settle down to an equilibritum point. Thus, the stability of the system may be concluded from this single scalar function without explicit knowledge of the actual solutions.[11] The energy function, $V(x)$ has two properties: 1) $V(x)$ is strictly positive unless both state variables x and $\dot{x}$ are zero, 2) the function is monotonically decreasing or $\dot{V}(x) \leq 0$. If $V(x)$ exists, then global stability can be inferred. The nonlinear rotational dynamics shown in Eq. 14 can be expanded and the constant coefficients can replaced by b, k_1, k_2, etc.

$$\ddot{\theta} + b\dot{\theta} + k_1\theta + k_2\theta^3 + k_2a_1\theta^2\dot{\theta} + k_2a_2\dot{\theta}^2\theta + k_2a_3\dot{\theta}^3 = 0 \tag{19}$$

since $\dot{\theta}^2 \geq 0$, $k_2a_2\dot{\theta}^2$ can be replaced with a positive time varying quantity, k_3

$$\ddot{\theta} + b\dot{\theta} + (k_1 + k_3)\theta + k_2\theta^3 + k_2a_1\theta^2\dot{\theta} + k_2a_3\dot{\theta}^3 = 0 \tag{20}$$

The form of Eq. 20 can be thought of as a nonlinear mass-spring-damper system. The Lyapunov function, V, can be represented as the total mechanical energy:

$$V(\theta, \dot{\theta}) = \frac{1}{2}\dot{\theta}^2 + \int_0^{\theta} (k_1 + k_3)\theta + k_2\theta^3 d\theta \tag{21}$$

$$V(\theta, \dot{\theta}) = \frac{1}{2}\dot{\theta}^2 + \frac{1}{2}(k_1 + k_3)\theta^2 + \frac{1}{4}k_2\theta^4 \tag{22}$$

The derivative of V can be obtained:

$$\dot{V}(\theta, \dot{\theta}) = \dot{\theta}\ddot{\theta} + (k_1 + k_3)\theta\dot{\theta} + k_2\theta^3\dot{\theta} \tag{23}$$

$$\dot{V}(\theta, \dot{\theta}) = \dot{\theta}[-b\dot{\theta} - (k_1 + k_3)\theta - k_2\theta^3 - k_2a_1\theta^2\dot{\theta} - k_2a_3\dot{\theta}^3] + (k_1 + k_3)\theta\dot{\theta} + k_2\theta^3\dot{\theta} \tag{24}$$

$$\dot{V}(\theta, \dot{\theta}) = -b\dot{\theta}^2 - k_2a_1\theta^2\dot{\theta}^2 - k_2a_3\dot{\theta}^4 \tag{25}$$

$\dot{V}$ is negative semi-definite, therefore V is considered to be a Lyapunov function for the system and the global stability of the pendulum limit cycle can be inferred.

V. Conclusion

In this work, a simplified planar dumbbell dynamics model in conjunction with a nonlinear C_N vs. α aerodynamics model served as the basis of an analytical investigation into the fundamental dynamics of pendulum motion for a two-parachute cluster system. Output error methodology from system identification theory was used to identify the parameters of the nonlinear aerodynamics model. The identified model yielded excellent comparison with portions of flight test data where the pendulum motion occurred. Due to the inherent nonlinear nature of the pendulum motion limit cycle, traditional nonlinear analysis techniques were applied to gain further insight into the system. Lyapunov's direct method provided mathematical proof in the absolute stability of the pendulum motion. Describing Function method was used to predict the amplitude and frequency of the limit cycle oscillation. Finally, the phase plane analysis was used to visualize the size and shape of the limit cycle with respect to variations in key aerodynamic parameters.

VI. Acknowledgements

This work was supported by the NASA Engineering Safefy Center (NESC). Flight testing, instrumentation, and data collection were performed at NASA Johnson Space Center. Best Estimated Trajectory (BET) files were provided by Phil Robinson. The reduced flight data and output-error code was provided by Eugene Morelli. Jessie Powell provided excellent insights into the CPAS parachute aerodynamics. Helpful technical reviews were performed by Dr. Eugene Morelli, Richard Barton, Dr. Carlos Roithmayr, and Daniel Murri.

References

[1]Ray, E. S., and Machín, R. A., "Pendulum Motion in Main Parachute Clusters," No. 2015-2138, AIAA, 2015.

[2]Ali, Y., Sommer, B., Troung, T., Anderson, B., and Madsen, C., "Orion Multi-Purpose Crew Vehicle Solving and Mitigating the Two Main Cluster Pendulum Problem." No. 2017-4056, *24rd Aerodynamic Decelerator Conference*. AIAA, 2017.

[3]White, F. M., and Wolf, D. F., "A Theory of Three-Dimensional Parachute Dynamic Stability," *Journal of Aircraft*, Vol. 5, No. 1, 1968, pp. 86–92.

[4]Ginn J. M., Clark, I. G., and Braun, R. D., "Parachute Dynamic Stability and the Effects of Apparent Inertia," No. 2014-2390, AIAA, 2014.

[5]Eaton, J. A., "Added Mass and the Dynamic Stability of Parachutes," *Journal of Aircraft*, Vol. 19, No. 5, 1982, pp. 414–416.

[6]Knacke, T. W., *Parachute Recovery Systems Design Manual*, Para Publications, Santa Barbara, 1991.

[7]Greathouse, J., and Schwing, A., "Study of Geometric Porosity and Drag using Computational Fluid Dynamics for Rigid Parachute Shapes." No. 2015-2131, *23rd Aerodynamic Decelerator Conference*. AIAA, 2015.

[8]Wolf, D., and Heindel, K., "A Steady Rotation Motion for a Cluster of Parachutes," No. 2005-1629, AIAA, 2005.

[9]Roithmayr, C., Beaty, J., Pei, J., Barton, R., and Matz, D., "Linear Analysis of a Two-Parachute System Undergoing Pendulum Motion," submitted, 25th Aerodynamic Decelerator Conference, AIAA, 2019.

[10]Morelli, A. E., and Klein, V., *Aircraft System Identification, Theory and Practice*, Sunflyte Enterprises, Williamsburg, VA. 2016.

[11]Slotine, E. J., and Li, W., *Applied Nonlinear Control*, Pearson Education, Upper Saddle River, NJ. 1991.

[12]Morelli, A. E., "System IDentification Programs for AirCraft (SIDPAC)". http://software.nasa.gov

[13]Pamadi, N. B., *Performance, Stability, Dynamics, and Control of Airplanes*, 3rd Ed, AIAA, 2015, pp. 427-428.

[14]Orr, J., "Stability and Flight Readiness of the SLS FCS with Adaptive Augmentation. Appendix D. Describing Function Analysis,". NESC report, 2016.